Science Advances
AAAS

advances.sciencemag.org/cgi/content/full/6/15/eaba1104/DC1

Supplementary Materials for

Cooperativity of $K_v7.4$ channels confers ultrafast electromechanical sensitivity and emergent properties in cochlear outer hair cells

Maria C. Perez-Flores, Jeong H. Lee, Seojin Park, Xiao-Dong Zhang, Choong-Ryoul Sihn, Hannah A. Ledford, Wenying Wang, Hyo Jeong Kim, Valeriy Timofeyev, Vladimir Yarov-Yarovoy, Nipavan Chiamvimonvat, Richard D. Rabbitt*, Ebenezer N. Yamoah*

*Corresponding author. Email: enyamoah@gmail.com (E.N.Y.); r.rabbitt@utah.edu (R.D.R.)

Published 8 April 2020, *Sci. Adv.* **6**, eaba1104 (2020)
DOI: 10.1126/sciadv.aba1104

This PDF file includes:

Supporting Information
Methods

Outer Hair Cell Mathematical Model

We modeled electro-mechanics of outer hair cells (OHCs) by coupling passive properties of the cell with a 4-state chemical kinetic model of $K_v7.4$ and a piezoelectric model of prestin-dependent motility. The approach is shown schematically in Supplementary (**S**)**5**. The piezoelectric coefficient was modeled as voltage-dependent, which gives rise to the signature nonlinear capacitance of the membrane (*25, 36*). Passive electrical capacitance of the membrane was assumed to act in parallel with the piezoelectric element and ionic conductances. To capture voltage, mechanical, and temperature sensitivity, $K_v7.4$ was modeled using four states and Eyring's transition state theory (*24*), with the first three states closed and the fourth state open. The enthalpy associated with the first two transitions (A, B) was modeled as voltage-dependent, while enthalpy of the final transition (B) was modeled as tension dependent. Oligomerization was modeled as reducing the entropy of the first transition (A), thus favoring closed state 2 over closed-state 1. The increase in kinetics with oligomerization arises in this model from the difference in kinetics between transitions. Single-channel kinetics requires the final transition to the open state to be much faster than voltage-dependent transitions between closed states (*37*).

A. 4-State $K_v7.4$ Model.

$K_v7.4$ data in the parent report can be described reasonably well using a simple chemical kinetic model. We formulated the 4-state model with the goal of simplicity, while maintaining thermodynamic consistency, understanding that transitions of the $K_v7.4$ channel are undoubtedly more complex (**S5**). Kinetics is modeled using

$$\frac{d\vec{p}}{dt} = \mathbf{K}\vec{p} \tag{1}$$

Where $\vec{p} = \begin{bmatrix} p_1 & p_2 & p_3 & p_4 \end{bmatrix}^T$ provides the probability that the subunit is in one of 4 states. The matrix $\mathbf{K}$ is a function of the thermodynamic (v, f, ξ, T) state variables and has the form

$$\mathbf{K} = \mathbf{K}(v, f, \xi, T) = \begin{bmatrix} -k_{12} & k_{21} & 0 & 0 \\ k_{12} & -(k_{21} + k_{23}) & k_{32} & 0 \\ 0 & k_{23} & -\left(k_{32} + k_{34}\right) & k_{43} \\ 0 & 0 & k_{34} & -k_{43} \end{bmatrix} \tag{2}$$

Where v is the membrane potential, f is membrane tension, ξ is oligomerization, and T is temperature. The membrane tension is related to the intracellular pressure and the load (Appendix A), thus linking tension acting on $K_v7.4$ channels to the mechanical load and tension in the lateral wall motor elements. At steady state

$$\begin{aligned} p_1^{\infty} &= k_{21}k_{32}k_{43}/c \\ p_2^{\infty} &= k_{12}k_{32}k_{43}/c \\ p_3^{\infty} &= k_{12}k_{23}k_{43}/c \\ p_4^{\infty} &= k_{12}k_{23}k_{34}/c \end{aligned} \tag{3}$$

where

$$c = k_{12}k_{23}k_{34} + k_{12}k_{23}k_{43} + k_{12}k_{32}k_{43} + k_{21}k_{32}k_{43} \tag{4}$$

The channel open probability is $P_O = P_4^h \approx \left(K_O P_3\right)^h$, where h is selected based on experimental observations. The whole-cell $K_v7.4$ current is

$$I_{Kn} = G_{Kn}^{\infty} P_4^h (v - E_K) \tag{5}$$

Voltage-sensitivity

The rate constants are modeled using Eyring's transition state theory

$$k_{nm} = \alpha_{nm} e^{-\Delta G_{nm}/RT} \tag{6}$$

where the Gibbs free energy ΔG is written in terms of the enthalpy ΔH, entropy ΔS, and the potential v through which the gating charge z moves

$$\Delta G_{nm} = \Delta H_{nm} - T\Delta S_{nm} - z_{nm}Fv \ . \quad (7)$$

Here, we define v the full membrane potential and adjust the gating charge accordingly. The half-activation voltage associated with transitions $C_1 \rightleftharpoons C_2$ & $C_2 \rightleftharpoons C_3$ is $\Phi_{nm} = \left(\Delta H_{nm} - T\Delta S_{nm}\right)/z_{nm}F$, allowing the Gibbs free energy to be written in the form $\Delta G_{nm} = \left(\Phi_{nm} - v\right)z_{nm}F$. Symmetry is assumed $z_{nm} = -z_{mn}$.

Oligomerization

Oligomerization is modeled as reducing the entropy associated with the first forward transition by a scaling factor $0 \le \xi \le 1.$ This enters into the Gibbs free energy of the first state transition

$$\begin{aligned} \Delta G_{12} &= \Delta H_{12} - (2-\xi)T\Delta S_{12} - z_{12}FV \\ \Delta G_{21} &= \Delta H_{21} - \xi T\Delta S_{21} + z_{12}FV \end{aligned} \quad (8)$$

In this model, oligomerization $(\xi < 1)$ increases the probability of the channel being in closed state 2 vs. closed state 1. This increases the speed of opening and shifts the voltage sensitivity in the hyperpolarized direction. Sensitivity to the parameter ξ is high, with data suggesting $0.95 < \xi \le 1.$

Thermo- and mechano-sensitivity

Temperature dependence is included directly in the model through modulation of all state transitions. One characteristic feature of voltage-gated K^+ channels is that the peak conductance increases with temperature even when the cell is highly depolarized, and voltage sensitivity is entirely saturated (*38*). This means temperature sensitivity must arise at a transition state downstream from the voltage-dependent transitions—this is the final transition in the present 4-state $K_v7.4$ model and previously published models of other channels (*37*). The final transition describes the kinetics of single-channel opening and hence is extremely fast with a transition time on the order of microseconds (*39*). The high speed of K^+ channel thermo-

sensitivity has been revealed previously in depolarized murine type II vestibular hair cells using infrared laser heat pulses (*40*). Analogous to temperature, present data demonstrate an increase in peak conductance with an increase in mechanical tension in the membrane even when the cell is highly depolarized, and $K_v7.4$ voltage sensitivity is saturated. In the present 4-state model, the only way to match the data is to place mechanical sensitivity downstream from voltage sensitivity at the final transition $C_3 \rightleftharpoons O_4$. This final transition to the open state is fast, so mechano-sensitivity in the present $K_v7.4$ model is also fast and capable of operating cycle-by-cycle at auditory frequencies. Mechano-sensitivity of transition "jk=34,43" is included by modulating the Gibbs free energy through the mechanical enthalpy

$$\Delta G_{jk} = \Delta H_{jk} - T\Delta S_{jk} \ . \tag{9}$$

The rate constants are assumed to be $k_{jk} = \alpha_{jk} e^{-\Delta G_{jk}/RT}$, giving the equilibrium constant $K_C = k_{34}/k_{43}$. In wild type outer hair cells, $K_v7.4$ channels are primarily in the basal pole of the cell, a location that senses the force between the motor element and the external load. Using a linear model, the stress in this region of the membrane is related to the whole-cell strain $\varepsilon = \varepsilon_0 + \varepsilon_1$, where ε_0 is the resting pre-strain (constant or slowly changing) and ε_1 is the perturbation (changing cycle-by-cycle). It's essential to recognize that the strain is whole-cell load-dependent, and hence mechanical gating in this model will depend on specifics of the loading, which change with frequency (also see Appendix A). In the present model, we assume small perturbations in strain about the resting state and model strain dependence of the equilibrium constant as a saturating sigmoid function

$$K_C = K_1 + \frac{K_2}{1 + e^{-\varepsilon_1/K_3}}, \tag{10}$$

Where K_1 , K_2 and K_3 are constants. The reverse rate k_{43} is defined using Eq. 9, and the strain-dependent forward rate is computed using $k_{34} = K_C k_{43}$.

B. Outer Hair Cell Electromechanics

Piezoelectric equations.

The composite hair cell membrane is modeled as a 1-D piezoelectric cylindrical shell with axial strain ε, membrane voltage v, and tension per unit membrane circumference f ($f = stress \cdot thickness$ N.m^{-1}). The whole-cell volume is assumed to remain constant, thus relating the axial strain to the circumferential strain (Appendix A). The whole-cell axial strain in the lateral wall is a superposition of strain in piezoelectric elements occupying area fraction φ plus strain in the passive elements occupying area fraction $(1-\varphi)$. We consider rapid motions where water transport is zero, and the cell volume is constant, thus providing a kinematic coupling between changes in length to changes in radius and membrane surface area. With this, the axial strain is related to the axial stress and voltage in the piezoelectric composite by

$$\begin{aligned} \varepsilon &= \left(\varphi_0 \kappa_p + (1-\varphi_0)\kappa_s\right) f - \varphi_0 \delta_p v \\ \varepsilon &= \kappa_C f - \delta_C v \end{aligned} \tag{11}$$

Where δ_p is the axial piezoelectric coefficient, κ_p is the compliance of the parallel piezoelectric component, and κ_s is the passive series compliance. Combining terms $\delta_C = \varphi_0 \delta_p$ is the effective axial piezoelectric coefficient of the cell and $\kappa_C = \left(\varphi_0 \kappa_p + (1-\varphi_0)\kappa_s\right)$ is the effective axial compliance of the cell.

Mechanical loading on the OHC relates the axial stress to the strain. Assuming the load arises from mass, stiffness, and viscosity of the cell itself plus the external load provides

$$m_L \frac{d^2\varepsilon}{dt^2} + \eta_L \frac{d\varepsilon}{dt} + k_L \varepsilon = f \frac{2\pi r}{\ell} + \frac{g}{\ell} \tag{12}$$

Where (m_L, η_L, k_L) are the effective mass, damping, and stiffness loading parameters, $g(t)$ is the externally applied force (if any)? r is the cell radius, and ℓ is the length. We use Eq. 15 to

eliminate the tension. For small changes in strain $\varepsilon = \varepsilon_0 + \varepsilon_1$ about the preloaded (turgor pressure) condition ε_0

$$m_T \frac{d^2\varepsilon_1}{dt^2} + \eta_T \frac{d\varepsilon_1}{dt} + k_T\varepsilon_1 - \left(k_C\delta_C\right)v = k_T\varepsilon_0 \ , \quad (13)$$

Where the intrinsic stiffness of the cell comes from the compliance according to $k_C = 2\pi r / \ell\kappa_C$, and $k_T\varepsilon_0 = k_C\delta_C V_0$ (note: the piezoelectric coefficient δ_C is a function of voltage). The subscript "T" denotes "total" coefficients that account for the external load plus the cell itself $\left(m_T = m_L + m_C, \eta_T = \eta_L + \eta_C, k_T = k_L + k_C\right)$. Written as first-order equations

$$\begin{aligned} \frac{d\varepsilon_1}{dt} &= \varepsilon_2 \\ \frac{d\varepsilon_2}{dt} &= -\frac{1}{m_T}\left(\eta_T\varepsilon_2 - k_T\varepsilon_1 - k_C\delta_C v + k_T\varepsilon_0 + g/\ell\right) \end{aligned} \quad (14)$$

The displacement current across the cell membrane is the addition of components in the piezoelectric material and the passive membrane

$$i_D = C_L\frac{dv}{dt} + \frac{A_p\varphi_0\delta_p}{\kappa_p}\frac{d\varepsilon_p}{dt} \quad (15)$$

Where A_p is the total membrane area containing piezoelectric elements, and C_L is the passive whole-cell capacitance ("linear capacitance"). The displacement current can be written as

$$i_D = \left(C_L + \frac{A_p\varphi_1\delta_C^2}{\kappa_C}\right)\frac{dv}{dt} - \left(\frac{A_p\varphi_0\delta_C}{\kappa_C}\right)\frac{d\varepsilon}{dt} \quad (16)$$

where the nondimensional fraction $\varphi_1 = \left(\frac{\kappa_s}{\kappa_p}(1-\varphi_0)\right)$.

From Kirchoff's current law, the whole-cell current is related to the membrane potential by

$$\left(C_L+\frac{\varphi_1 A_p \delta_C^2}{\kappa_C}\right)\frac{dv}{dt}-\left(\frac{\varphi_0 A_p \delta_C}{\kappa_C}\right)\frac{d\varepsilon}{dt}+\sum_{j=1}^{N} i_j = i \tag{17}$$

where i_j are the membrane currents, i is the whole-cell injected current (including the MET current).

Nonlinear Capacitance

In general, the nonlinear part of the capacitance depends on the load. Two limiting cases are of interest and arise directly from Eq. 21: the zero-strain case

$$C_{NL}\big|_{S=0} = \frac{\varphi_1 A_p \delta_C^2}{\kappa_C} \ , \tag{18}$$

and the zero-force case

$$C_{NL}\big|_{f=0} = \frac{\left(\varphi_0+\varphi_1\right) A_p \delta_C^2}{\kappa_C} \ . \tag{19}$$

Note, the nonlinear capacitance approaches zero in the zero-strain case only if the compliance of the passive component of the membrane is zero ($\varphi_1 \to 0$ Eq. 22). In general, the prestin-dependent piezoelectric coefficient is voltage, strain, and temperature-dependent $\delta_C = \delta_C\left(v,\varepsilon,\Theta\right)$. Simulations reported in the present study consider small perturbations about a resting strain ε_0 and temperature Θ_0 and assume voltage dependence of the piezoelectric coefficient follows the conventional Boltzmann form (*25, 36*)

$$\delta_C = 4\delta_C^0\left\{e^{(v-v_{pk})/\lambda_{pk}}\left(1+e^{-(v-v_{pk})/\lambda_{pk}}\right)^2\right\}^{-1} \ . \tag{20}$$

Numerical simulations reported in the present report use Eq. 24, but for small perturbations in voltage about a resting value, it is sufficient to treat δ_C as a constant.

Hair cell currents

To examine the contribution of $K_v7.4$ to hair cell electromotility, in the present simulations we include only a passive conductance G_L, a prescribed MET current I_{MET}, and a voltage-strain dependent $K_v7.4$ conductance G_{Kn}

$$\sum_{j=1}^{N} i_j = G_L(V - E_L) + G_{Kn}^{\infty} P_4^h (V - E_K) + ... + I_{MET} \tag{21}$$

Simulations and OHC Model Parameters.

All simulations shown in the parent manuscript were based on data from OHCs in the ~3 kHz region of the cochlea. Parameters used in the simulations are provided in Table 1. Eqs. 5 and 21 were solved numerically in the time domain (Mathematica) under voltage-clamp conditions with zero MET current (simulating voltage-clamp experiments) and in response to 100pA sinusoidal MET current injection (simulating physiological conditions). The model is nonlinear. Simulations shown in the frequency domain determine the magnitude and phase of the response (voltage, displacement) based on first-harmonic time-domain modulation.

S Table 1. Model Physical Parameters

Parameter	Symbol	Value	Units
Area: Total Membrane	A_m	$\pi r\left(2\ell + 3r\right)$	m^2
Area: Lateral Wall	A_p	$2\pi r\ell$	m^2
Capacitance: linear	C_L	$0.0175 A_m$	F
Compliance: cell	κ_C	$1/(hk_0)$	$m.N^{-1}$
Compliance: piezo	κ_p	$\kappa_C / (\varphi_0 + (1-\varphi_0)/r_\kappa)$	$m.N^{-1}$
Compliance: ratio	r_κ	1	-
Damping: total	η_T	$2\sqrt{k_T m_T}$	$N.m^{-1}s^{-1}$
Density	ρ	1000	$kg.m^3$
Entropy: 12,21	$\Delta S_{12}, \Delta S_{21}$	227.9	Joule
Entropy: 23,32	$\Delta S_{23}, \Delta S_{32}$	22.8	Joule
Entropy: clustering	ξ	0.98	-
Faraday const.	F	96485.33	$s.A.mol^{-1}$
Fraction area	φ_0	0.9	-
Fraction stiffness	φ_1	$(1-\varphi_0)/r_k$	-
Frequency: ω_n	ω_n	4000	Hz
Gas const.	R	8.3145	$J.mol\text{-}^{1.\circ}K^{-1}$
Half activation: 12,21	Φ_{12}, Φ_{21}	-0.05	V
Half activation: 23,32	Φ_{23}, Φ_{32}	-0.06	V
Length of lateral wall	ℓ	25e-6	m
Mass: total	m_T	k_T / ω_n^2	Kg
Mech. Gating: 1	K_1	10	-
Mech. Gating: 2	K_2	-8	-

Mech. Gating: 3	K_3	1e-4	-
Piezo.: coef.	δ_p^0	-1.4	V^{-1}
Piezo.: V width	λ_{pk}	0.0389	-
Piezo.: V peak	v_{pk}	-0.040	V
Radius of OHC	r	5e-6	m
Resting potential	v_0	-0.055	V
Resting strain	ε_0	$\delta_C(v_0)v_0k_C / k_T$	-
Reversal: K^+	E_K	-0.07	V
Rate: 12, 21	α_{12}, α_{21}	75	s^{-1}
Rate: 23, 32	α_{23}, α_{32}	225	s^{-1}
Rate: 43, 43	α_{34}, α_{43}	3750	s^{-1}
Stiffness: Reference	k_0	1e6	$N.m^{-2}$
Stiffness: cell	k_C	$2\pi r / (\ell \kappa_C)$	$N.m^{-1}$
Stiffness: total	k_T	$1.25k_C$	$N.m^{-1}$
Temperature	T	283.15	°K
Thickness: Reference	h	1e-8	m

Appendix 1. Kinematics

For a piezoelectric shell, the strains ε_n in the axial and circumferential directions are related to the tensile forces f_n (stress times thickness) and in the membrane and the voltage V by

$$\begin{aligned} \varepsilon_1 &= \kappa_{11} f_1 + \kappa_{12} f_2 + \delta_1 V \quad (a) \\ \varepsilon_2 &= \kappa_{21} f_1 + \kappa_{22} f_2 + \delta_2 V \quad (b) \end{aligned} \tag{A1}$$

Assuming constant volume cycle-by-cycle deformations of a cylinder requires $\varepsilon_2 = -\varepsilon_1 / 2$. Substitution into Eq. A1 provides the equivalent 1-D piezoelectric model for the axial strain in the OHC

$$\begin{aligned} \varepsilon_1 &= \left(\kappa_{11} - \frac{\kappa_{12}(\kappa_{11} + 2\kappa_{21})}{(\kappa_{22} + 2\kappa_{12})} \right) f_1 + \left(\delta_1 + \frac{\kappa_{12}(\delta_1 + 2\delta_2)}{(\kappa_{22} + 2\kappa_{12})} \right) V, \quad (a) \\ \varepsilon &= \kappa f + \delta V, \quad (b) \end{aligned} \tag{A2}$$

Where Eq. A2b is the axial piezoelectric model used in Eq. 11. Notice, constant-volume cylindrical kinematics has the effect of decreasing the effective axial stiffness while increasing the effective piezoelectric constant. OHCs are under intracellular pressure consisting of a static turgor pressure plus a perturbation $P = P_0 + P'$. The extracellular pressure on the outside of the lateral wall is set to zero, thus by Laplace's law requiring $f_2 = rP$. The external load is modeled as a pressure P_{load} on the end caps of the OHC, by static force balance requiring $f_1 = r(P - P_{load})/2$, where the external pressure is related to the external force by $P_{load} = 2 f_{load} / r$. Modulation of the strain and force by action against an external load at the ends of the cell also modulates the intracellular pressure and the force acting on the motor element along the lateral wall as well as the force acting on $K_v7.4$.

S1. Developmental changes in time constant of activation of linopirdine (lino)-sensitive K^+ current in OHCs. The time constant of activation of the lino-sensitive currents against activation voltages (P8 ○, P24, ●) (n = 24, for P8 and P24). Data were assembled from OHCs located at 3-4 kHz region of the cochlea.

S2. $K_v7.4$ and fusion CIBN-EGFP-$K_v7.4$ channels have similar properties. a-b, Current traces recorded from HEK 293 cells transfected with EGFP-$K_v7.4$. a, traces in black) and CIBN-EGFP-$K_v7.4$ (b, traces in green). Cells were held at -80 mV and stepped from -120 to 60 mV, using 10-mV increments. The tail current was generated at -30 mV. c, Current density-voltage (I-V) relation of data obtained from 17 cells in each group (color-coded as in **a** and **b**). **d,** Voltage-dependence of the steady-state activation was fitted with a single Boltzmann function. The half-activation voltage ($V_{1/2}$) and the voltage sensitivity at half-activation (1/k, (V^{-1})) derived for EGFP-$K_v7.4$ and CIBN-EGFP-$K_v7.4$ currents were, -15.2 $\pm$ 1.2 mV and 76.3 $\pm$ 12.4 V^{-1}; and -17.2 $\pm$ 2.7 mV and 84.0 $\pm$ 12.2 V^{-1}, (n = 17), respectively. Comparing the $V_{1/2}$ and 1/k for EGFP-$K_v7.4$ and CIBN-EGFP-$K_v7.4$ currents ($V_{1/2}$, p = 0.01 and 1/k, p = 0.08). **e.** Images of representative HEK 293 cells transfected with CIBN-GFP-$K_v7.4$ and CRY2-mCherry in the dark (left panel) and 5-min after exposure to blue light to induce CIBN-CRY2 dimerization. Scale bars represent 5-μm. **f,** (Upper panel) activation of CIBN-EGFP-$K_v7.4$ channels before (black trace) and after 4-min blue light exposure (blue trace). Light- and voltage-pulse protocols are shown in the left inset. Holding, step and deactivation/tail voltages were -80, 0, and -40 mV. The right inset is an expanded view of the test-pulse (p2) elicited current before and after blue light exposure. Lower panel shows similar current records from CIBN-EGFP-$K_v7.4$ and CRY2-mCherry co-expressed cells. Of note, blue light exposure and by extension, induction of channel clusters sped up the current onset and mediated faster activation kinetics.

S3. Acute application of hypertonic solution did not visibly alter $K_v7.4$ expression in OHCs. a Expression pattern of $K_v7.4$ in OHCs from P21 mice. Hair cells were labelled with myosin 7A antibody (Alexa 488 or FITC in green) and $K_v7.4$ antibody (Alexa 555, in red). Nuclei were stained with Dapi (in blue). The merged image is shown (left panel). **b,** 5 min after application of 630 mmOsmol mannitol solution, the distribution of $K_v7.4$ remained infra-nuclear in OHCs (n = 210 OHCs from 3 different cochleae). **Scale bar = 5 μm.**

S4. Effects of prestin (*Slc26a5* encoding gene) and membrane tension on the properties of I_{Kn} and expression of $K_v7.4$. a, I_{Kn} traces recorded from *Slc26a5*$^{+/+}$ OHC (black traces) from a holding potential of -60 mV to step potentials ranging from -130 to 60 mV using voltage increment of 15-mV steps. Similar recording conditions from *Slc26a5*$^{-/-}$ OHC (blue traces). **b,** The steady-state activation curves were generated from the tail currents and fitted with a Boltzmann function; the $V_{1/2}$ for I_{Kn} in *Slc26a5*$^{+/+}$ OHC was -72.3 ± 1.3 mV and the voltage sensitivity at half-activation, 1/k, was 133.3 ± 11.6 V^{-1} and for *Slc26a5*$^{-/-}$ OHC was -48.2 ± 0.6 mV and the 1/k was 86.2 ± 9.8 V^{-1} (n = 7). Comparing $V_{1/2}$ and 1/k, $p < 0.0001$. **c,** Changes in the τ_{act} relative to step voltage for I_{Kn} in *Slc26a5*$^{+/+}$ (black) and *Slc26a5*$^{-/-}$ (blue) OHC (n = 7). **d,** the Expression pattern of $K_v7.4$ in OHCs from P21 *Slc26a5*$^{+/+}$ (left two panels) and *Slc26a5*$^{-/-}$ (right two panels) mice. Outer hair cells were labeled with myosin 7A antibody (Alexa 488 or FITC in green) and $K_v7.4$ antibody (Alexa 555, in red). In *Slc26a5*$^{-/-}$ OHCs, the distribution of $K_v7.4$ is scattered and supra-nuclear compared to the basolateral infra-nuclear consolidation in *Slc26a5*$^{+/+}$ OHCs. Shown with white X are sites of lost OHCs in *Slc26a5*$^{-/-}$ cochlea.

S5. $K_v7.4$ OHC model. a, The mechanical portion of the model with the cochlear load on the OHC represented as a spring-mass-damper (k_L,m_L,η_L) system. Electromotility is modeled as a voltage-dependent piezoelectric element (δ_p) in parallel with passive compliance (κ_p). The

contractile element acts in series with passive compliance (κ_s). Modulation of turgor pressure and membrane tension depend on contraction and the load, causing the mechanical force acting on $K_v7.4$ to depend on frequency and loading conditions. **b,** A whole-cell model including MET current input, voltage-dependent piezoelectric charge displacement (C_{NL}), passive linear capacitance (C_L), the $K_v7.4$ conductance, and other ion channels. **c,** A simple 4-state $K_v7.4$ model based on Eyring's transition state theory. The $K_v7.4$ open probability is modulated by the Gibbs free energy of each transition accounting for voltage, clustering, temperature, and mechanical tension in the membrane. **d-h,** Voltage clamp simulations for $K_v7.4$ transfected HEK cells: **d,** control condition, **e-f,** with blue light to evoke clustering, and **g,** with mechanical stress applied. **h,** Voltage sensitivity of the peak current ($I / I_{\max}$) for control (black), clustered (blue) and stressed (red) conditions.

S1

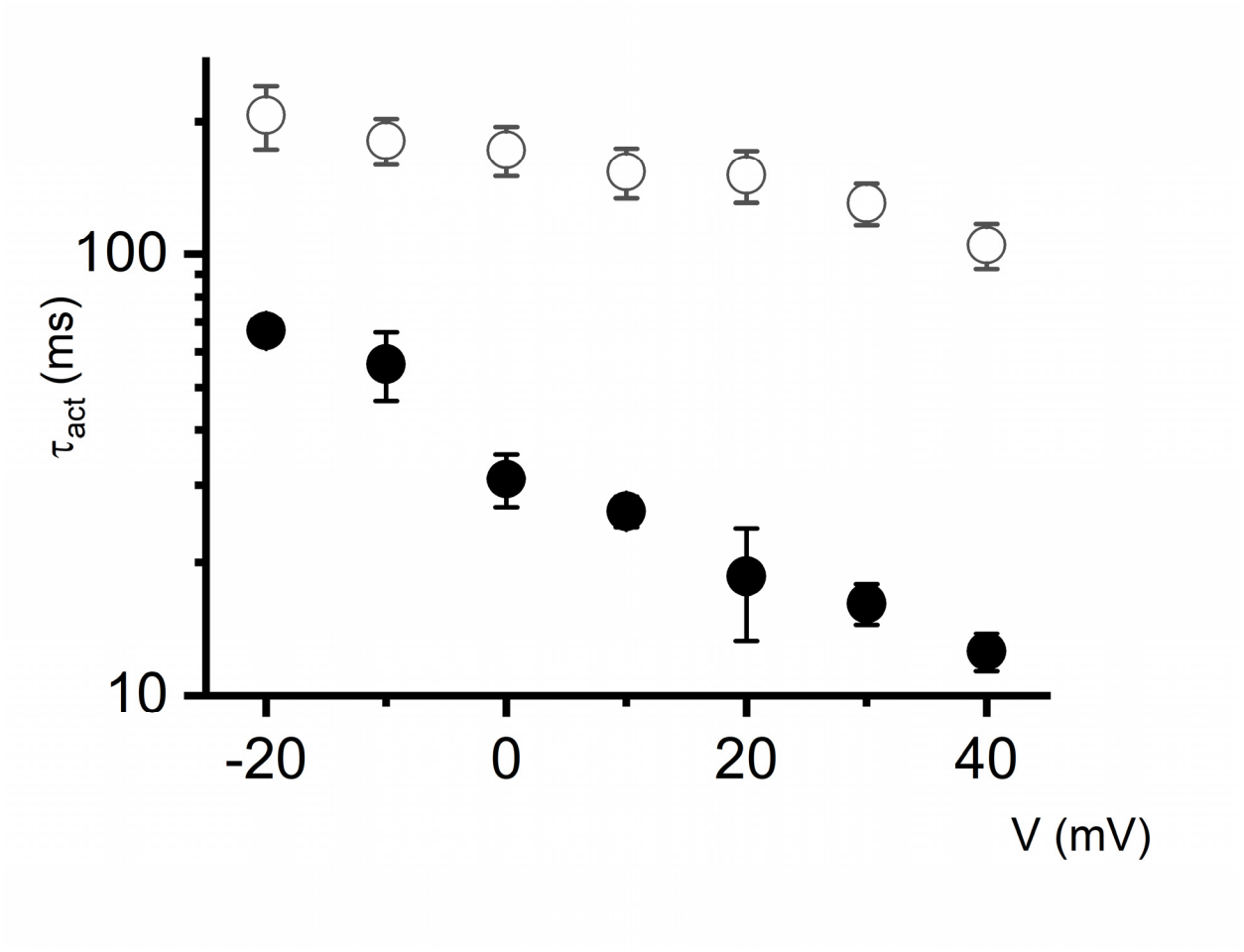

S2

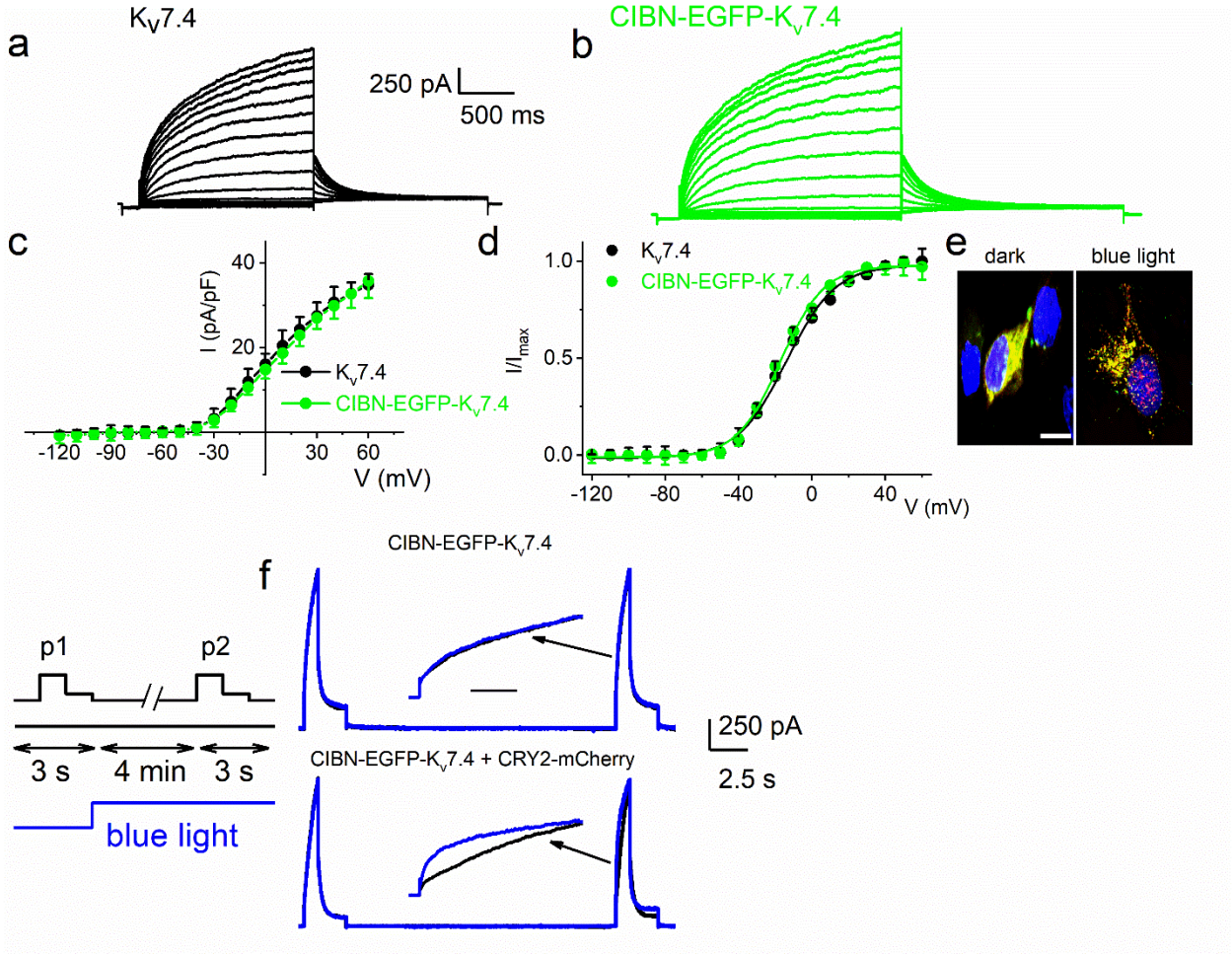
a
K_V7.4
250 pA
500 ms
b
CIBN-EGFP-K_V7.4
c
I (pA/pF)
40
20
-120 -90 -60 -30 30 60
V (mV)
K_V7.4
CIBN-EGFP-K_V7.4
d
I/I_{max}
1.0
0.5
0.0
-120 -80 -40 0 40
V (mV)
K_V7.4
CIBN-EGFP-K_V7.4
e
dark
blue light
f
CIBN-EGFP-K_V7.4
p1
p2
3 s
4 min
3 s
blue light
CIBN-EGFP-K_V7.4 + CRY2-mCherry
250 pA
2.5 s

S3

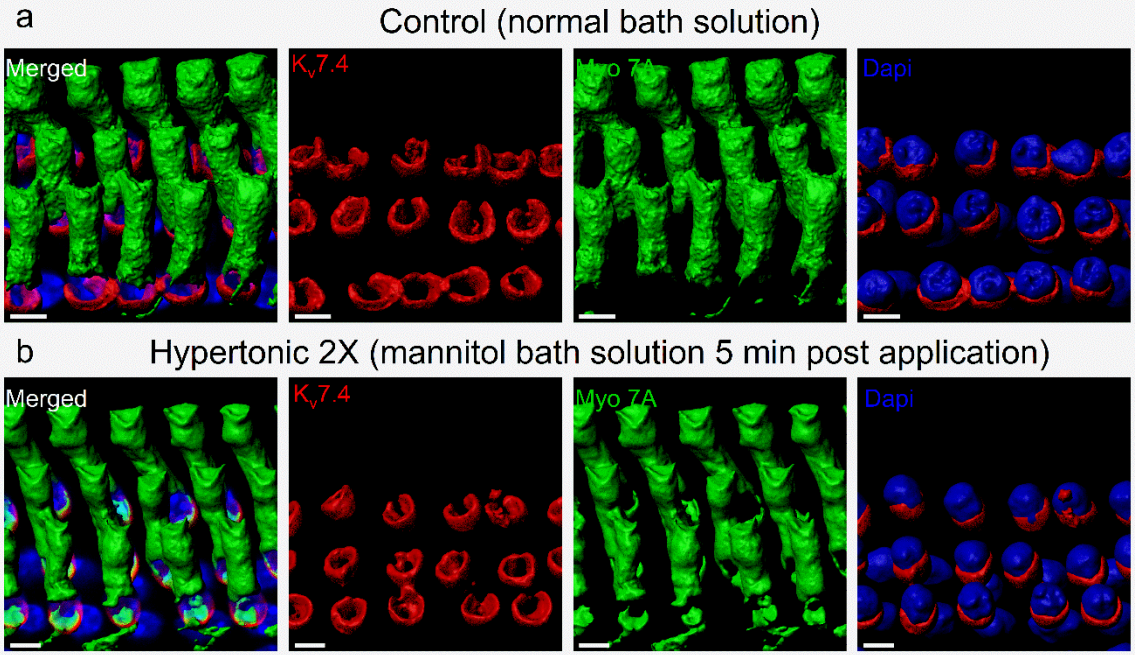
a
Control (normal bath solution)
Merged
$K_v7.4$
Myo 7A
Dapi
b
Hypertonic 2X (mannitol bath solution 5 min post application)
Merged
$K_v7.4$
Myo 7A
Dapi

S4

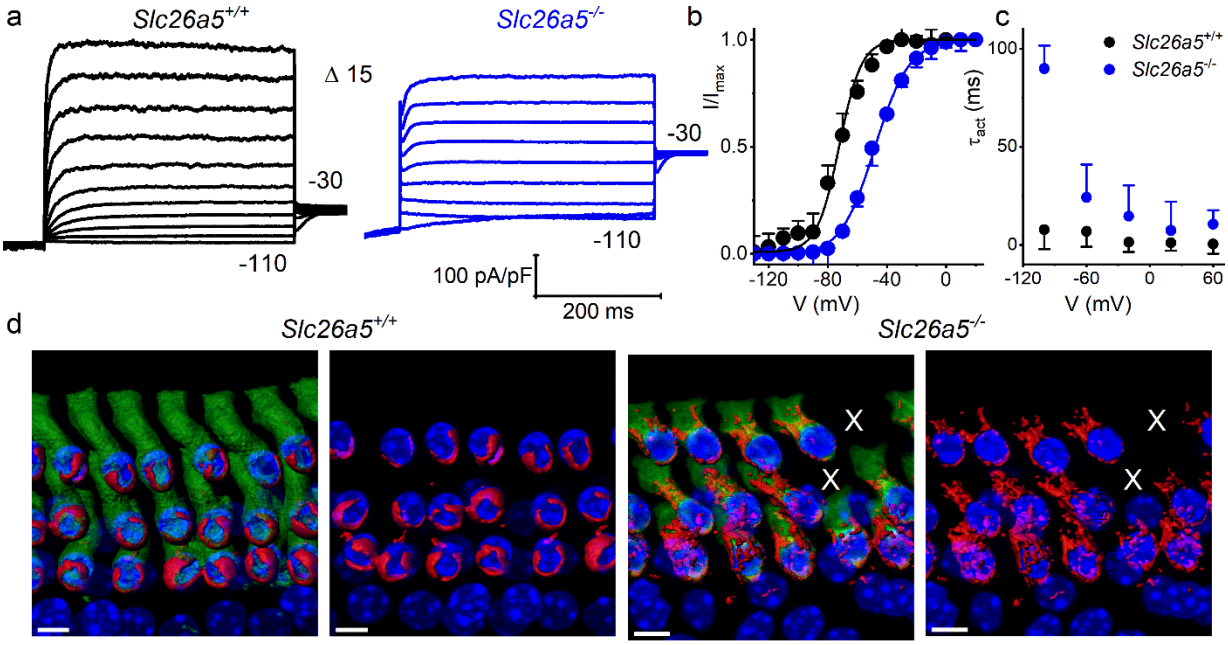
a
Slc26a5+/+
Slc26a5-/-
Δ 15
-30
-110
-30
-110
100 pA/pF
200 ms
b
I/Imax
1.0
0.5
0.0
-120
-80
-40
0
V (mV)
c
τact (ms)
100
50
0
-120
-60
0
60
V (mV)
Slc26a5+/+
Slc26a5-/-
d
Slc26a5+/+
Slc26a5-/-
X
X
X
X

S5

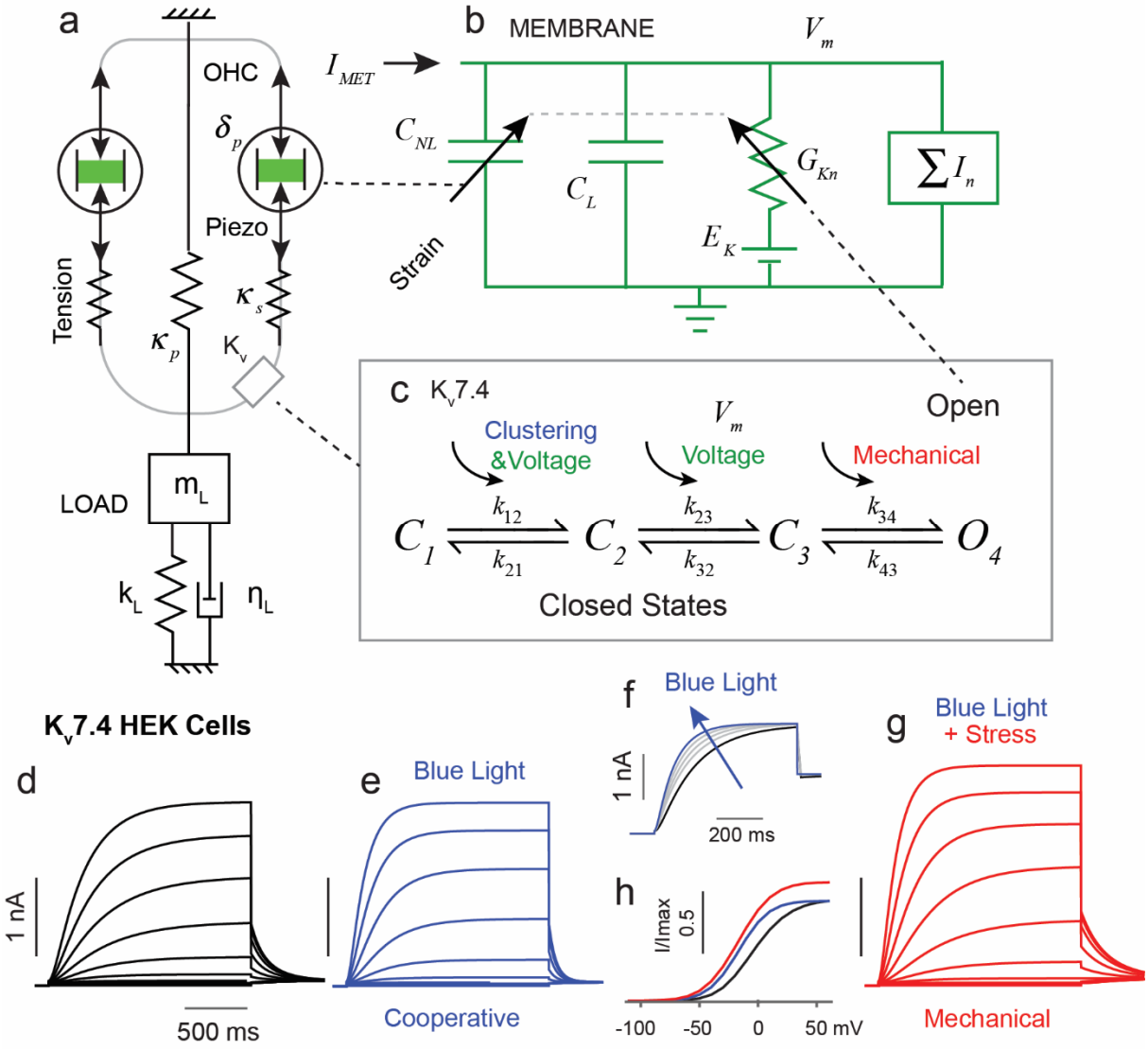
a
OHC
δ_p
Piezo
Tension
κ_p
κ_s
K_v
LOAD
m_L
k_L
η_L
b
MEMBRANE
V_m
I_{MET}
C_{NL}
C_L
G_{Kn}
$\sum I_n$
E_K
Strain
c K_v7.4
Open
V_m
Clustering &Voltage
Voltage
Mechanical
$C_1 \rightleftharpoons C_2 \rightleftharpoons C_3 \rightleftharpoons O_4$
k_{12} k_{21} k_{23} k_{32} k_{34} k_{43}
Closed States
K_v7.4 HEK Cells
d
1 nA
500 ms
e
Blue Light
Cooperative
f
Blue Light
1 nA
200 ms
g
Blue Light
+ Stress
Mechanical
h
I/Imax
0.5
-100
-50
0
50 mV

REFERENCES AND NOTES

1. C. E. Carr, C. Köppl, Coding interaural time differences at low best frequencies in the barn owl. *J. Physiol. Paris* **98**, 99–112 (2004).

2. W. E. Brownell, C. R. Bader, D. Bertrand, Y. de Ribaupierre, Evoked mechanical responses of isolated cochlear outer hair cells. *Science* **227**, 194–196 (1985).

3. G. Frank, W. Hemmert, A. W. Gummer, Limiting dynamics of high-frequency electromechanical transduction of outer hair cells. *Proc. Natl. Acad. Sci. U.S.A.* **96**, 4420–4425 (1999).

4. N. P. Cooper, A. Vavakou, M. van der Heijden, Vibration hotspots reveal longitudinal funneling of sound-evoked motion in the mammalian cochlea. *Nat. Commun.* **9**, 3054 (2018).

5. J. Santos-Sacchi, K. H. Iwasa, W. Tan, Outer hair cell electromotility is low-pass filtered relative to the molecular conformational changes that produce nonlinear capacitance. *J. Gen. Physiol.* **151**, 1369–1385 (2019).

6. J. Santos-Sacchi, W. Tan, The frequency response of outer hair cell voltage-dependent motility is limited by kinetics of prestin. *J. Neurosci.* **38**, 5495–5506 (2018).

7. J. Zheng, W. Shen, D. Z. Z. He, K. B. Long, L. D. Madison, P. Dallos, Prestin is the motor protein of cochlear outer hair cells. *Nature* **405**, 149–155 (2000).

8. A. J. Hudspeth, The cellular basis of hearing: The biophysics of hair cells. *Science* **230**, 745–752 (1985).

9. A. J. Ricci, H. J. Kennedy, A. C. Crawford, R. Fettiplace, The transduction channel filter in auditory hair cells. *J. Neurosci.* **25**, 7831–7839 (2005).

10. D. C. Mountain, A. E. Hubbard, A piezoelectric model of outer hair cell function. *J. Acoust. Soc. Am.* **95**, 350–354 (1994).

11. H. Davis, An active process in cochlear mechanics. *Hear. Res.* **9**, 79–90 (1983).

12. D. T. Kemp, Stimulated acoustic emissions from within the human auditory system. *J. Acoust. Soc. Am.* **64**, 1386–1391 (1978).

13. S. L. Johnson, M. Beurg, W. Marcotti, R. Fettiplace, Prestin-driven cochlear amplification is not limited by the outer hair cell membrane time constant. *Neuron* **70**, 1143–1154 (2011).

14. W. Marcotti, C. J. Kros, Developmental expression of the potassium current IK,n contributes to maturation of mouse outer hair cells. *J. Physiol.* **520**, 653–660 (1999).

15. T. Kharkovets, K. Dedek, H. Maier, M. Schweizer, D. Khimich, R. Nouvian, V. Vardanyan, R. Leuwer, T. Moser, T. J. Jentsch, Mice with altered KCNQ4 K^+ channels implicate sensory outer hair cells in human progressive deafness. *EMBO J.* **25**, 642–652 (2006).

16. A. Taslimi, J. D. Vrana, D. Chen, S. Borinskaya, B. J. Mayer, M. J. Kennedy, C. L. Tucker, An optimized optogenetic clustering tool for probing protein interaction and function. *Nat. Commun.* **5**, 4925 (2014).

17. M. J. Kennedy, R. M. Hughes, L. A. Peteya, J. W. Schwartz, M. D. Ehlers, C. L. Tucker, Rapid blue-light–mediated induction of protein interactions in living cells. *Nat. Methods* **7**, 973–975 (2010).

18. R. E. Dixon, C. Yuan, E. P. Cheng, M. F. Navedo, L. F. Santana, Ca^{2+} signaling amplification by oligomerization of L-type $Ca_v1.2$ channels. *Proc. Natl. Acad. Sci. U.S.A.* **109**, 1749–1754 (2012).

19. M. E. Gomez-Casati, E. Katz, E. Glowatzki, M. I. Lioudyno, P. Fuchs, A. B. Elgoyhen, Linopirdine blocks α9α10-containing nicotinic cholinergic receptors of cochlear hair cells. *J. Assoc. Res. Otolaryngol.* **5**, 261–269 (2004).

20. M. G. Leitner, A. Feuer, O. Ebers, D. N. Schreiber, C. R. Halaszovich, D. Oliver, Restoration of ion channel function in deafness-causing KCNQ4 mutants by synthetic channel openers. *Br. J. Pharmacol.* **165**, 2244–2259 (2012).

21. H. J. Kim, P. Lv, C.-R. Sihn, E. N. Yamoah, Cellular and molecular mechanisms of autosomal dominant form of progressive hearing loss, DFNA2. *J. Biol. Chem.* **286**, 1517–1527 (2011).

22. O. Yifrach, R. MacKinnon, Energetics of pore opening in a voltage-gated K^+ channel. *Cell* **111**, 231–239 (2002).

23. J.-M. Chambard, J. F. Ashmore, Regulation of the voltage-gated potassium channel KCNQ4 in the auditory pathway. *Pflügers Arch.* **450**, 34–44 (2005).

24. H. Eyring, The activated complex in chemical reactions. *J. Chem. Phys.* **3**, 107–115 (1935).

25. R. D. Rabbitt, S. Clifford, K. D. Breneman, B. Farrell, W. E. Brownell, Power efficiency of outer hair cell somatic electromotility. *PLOS Comput. Biol.* **5**, e1000444 (2009).

26. D. Ó Maoiléidigh, A. J. Hudspeth, Effects of cochlear loading on the motility of active outer hair cells. *Proc. Natl. Acad. Sci. U.S.A.* **110**, 5474–5479 (2013).

27. S. S. Gao, R. Wang, P. D. Raphael, Y. Moayedi, A. K. Groves, J. Zuo, B. E. Applegate, J. S. Oghalai, Vibration of the organ of Corti within the cochlear apex in mice. *J. Neurophysiol.* **112**, 1192–1204 (2014).

28. G. E. Kim, L. K. Kaczmarek, Emerging role of the KCNT1 Slack channel in intellectual disability. *Front. Cell. Neurosci.* **8**, 209 (2014).

29. C. M. Moreno, R. E. Dixon, S. Tajada, C. Yuan, X. Opitz-Araya, M. D. Binder, L. F. Santana, Ca^{2+} entry into neurons is facilitated by cooperative gating of clustered $Ca_V1.3$ channels. *eLife* **5**, e15744 (2016).

30. J. P. Dekker, G. Yellen, Cooperative gating between single HCN pacemaker channels. *J. Gen. Physiol.* **128**, 561–567 (2006).

31. D. J. Jagger, J. F. Ashmore, Regulation of ionic currents by protein kinase A and intracellular calcium in outer hair cells isolated from the guinea-pig cochlea. *Pflügers Arch.* **437**, 409–416 (1999).

32. T. Gold, Hearing. II. The physical basis of the action of the cochlea. *Proc. R. Soc. Lond. B Biol. Sci.* **135**, 492–498 (1997).

33. J. Ashmore, Biophysics of the cochlea—Biomechanics and ion channelopathies. *Br. Med. Bull.* **63**, 59–72 (2002).

34. S. T. Neely, D. O. Kim, A model for active elements in cochlear biomechanics. *J. Acoust. Soc. Am.* **79**, 1472–1480 (1986).

35. I. A. Belyantseva, G. I. Frolenkov, J. B. Wade, F. Mammano, B. Kachar, Water permeability of cochlear outer hair cells: Characterization and relationship to electromotility. *J. Neurosci.* **20**, 8996–9003 (2000).

36. J. Santos-Sacchi, Reversible inhibition of voltage-dependent outer hair cell motility and capacitance. *J. Neurosci.* **11**, 3096–3110 (1991).

37. R. Latorre, G. Vargas, G. Orta, S. Brauchi, Voltage and temperature gating of thermoTRP channels, in *TRP Ion Channel Function in Sensory Transduction and Cellular Signaling Cascades*, W. Liedtke, S. Heller, Eds. (CRC Press/Taylor & Francis, 2007), chap. 21.

38. F. Yang, J. Zheng, High temperature sensitivity is intrinsic to voltage-gated potassium channels. *eLife* **3**, e03255 (2014).

39. W. Y. Yang, M. Gruebele, Folding at the speed limit. *Nature* **423**, 193–197 (2003).

40. R. D. Rabbitt, A. M. Brichta, H. Tabatabaee, P. J. Boutros, J. Ahn, C. C. Della Santina, L. A. Poppi, R. Lim, Heat pulse excitability of vestibular hair cells and afferent neurons. *J. Neurophysiol.* **116**, 825–843 (2016).